Cancer Research

AACR

An Essential Requirement for the SCAP/SREBP Signaling Axis to Protect Cancer Cells from Lipotoxicity

Kevin J. Williams, Joseph P. Argus, Yue Zhu, et al.

Updated version	Access the most recent version of this article at: doi:10.1158/0008-5472.CAN-13-0382-T
Supplementary Material	Access the most recent supplemental material at: http://cancerres.aacrjournals.org/content/suppl/2013/02/25/0008-5472.CAN-13-0382-T.DC1.html

Cited Articles	This article cites by 35 articles, 15 of which you can access for free at: http://cancerres.aacrjournals.org/content/73/9/2850.full.html#ref-list-1

E-mail alerts	Sign up to receive free email-alerts related to this article or journal.
Reprints and Subscriptions	To order reprints of this article or to subscribe to the journal, contact the AACR Publications Department at pubs@aacr.org.
Permissions	To request permission to re-use all or part of this article, contact the AACR Publications Department at permissions@aacr.org.

An Essential Requirement for the SCAP/SREBP Signaling Axis to Protect Cancer Cells from Lipotoxicity

Kevin J. Williams[1,5], Joseph P. Argus[5,7], Yue Zhu[5,7], Moses Q. Wilks[4], Beth N. Marbois[1,5], Autumn G. York[5,6,7], Yoko Kidani[1,5], Alexandra L. Pourzia[1,5], David Akhavan[7], Dominique N. Lisiero[7], Evangelia Komisopoulou[6,7], Amy H. Henkin[5,7], Horacio Soto[3], Brian T. Chamberlain[8,11], Laurent Vergnes[2], Michael E. Jung[8,11], Jorge Z. Torres[9], Linda M. Liau[3,10], Heather R. Christofk[5,7,10], Robert M. Prins[3,10], Paul S. Mischel[12,13,14], Karen Reue[2,8], Thomas G. Graeber[5,6,7,10], and Steven J. Bensinger[1,5,7,10]

Abstract

The sterol regulatory element-binding proteins (SREBP) are key transcriptional regulators of lipid metabolism and cellular growth. It has been proposed that SREBP signaling regulates cellular growth through its ability to drive lipid biosynthesis. Unexpectedly, we find that loss of SREBP activity inhibits cancer cell growth and viability by uncoupling fatty acid synthesis from desaturation. Integrated lipid profiling and metabolic flux analysis revealed that cancer cells with attenuated SREBP activity maintain long-chain saturated fatty acid synthesis, while losing fatty acid desaturation capacity. We traced this defect to the uncoupling of fatty acid synthase activity from stearoyl-CoA desaturase 1 (SCD1)–mediated desaturation. This deficiency in desaturation drives an imbalance between the saturated and monounsaturated fatty acid pools resulting in severe lipotoxicity. Importantly, replenishing the monounsaturated fatty acid pool restored growth to SREBP-inhibited cells. These studies highlight the importance of fatty acid desaturation in cancer growth and provide a novel mechanistic explanation for the role of SREBPs in cancer metabolism. *Cancer Res; 73(9); 2850–62. ©2013 AACR.*

Introduction

Metabolic reprogramming has emerged as a defining feature of many cancer types (1). More than 80 years ago, Otto Warburg described increased consumption of glucose and production of lactate by cancer cells under normoxic conditions (2). Preferential use of aerobic glycolysis (termed as Warburg effect) in cancer cells can confer a significant growth and survival advantage to rapidly dividing cells by providing carbons, ATP, and reducing equivalents necessary to meet the anabolic demands of dysregulated growth (3, 4). Likewise, increased amino acid consumption (e.g., glutamine), perturbed mitochondrial function, and altered lipid metabolic programs can also contribute to the biosynthetic and bioenergetic demands of rapidly dividing cancer cells in the tumor microenvironment (5, 6). Although it is clear that dysregulated metabolism is an important characteristic of cancer cell biology, the molecular programs that support the cancer metabolic phenotype have yet to be fully understood.

The sterol regulatory element-binding proteins (SREBP1 and 2) are bHLH-zip transcription factors that have a well-defined role in regulating lipid homeostasis (7). SREBP1c preferentially regulates genes involved in fatty acid metabolism, whereas SREBP2 principally controls expression of genes involved in lipoprotein uptake and *de novo* sterol synthesis (8, 9). The SREBP1a isoform efficiently drives fatty acid and sterol biosynthesis as well as lipoprotein uptake by transactivating both SREBP1 and SREBP2 target genes. SREBPs are subject to complex posttranslational regulation. Goldstein and colleagues have delineated an elegant sterol-sensitive model of SREBP regulation in the endoplasmic reticulum (10). Immature (inactive) SREBP proteins are embedded in the endoplasmic reticulum membrane in association with 2 chaperone proteins INSIG and SCAP. Both SCAP and INSIG have sterol-sensing domains that bind endoplasmic reticulum membrane cholesterol or oxysterols and are exquisitely sensitive to alterations in endoplasmic reticulum membrane sterol levels. A small reduction in endoplasmic reticulum membrane sterol levels alters INSIG and SCAP conformation, resulting in the release of the SCAP/SREBP complex from INSIG (11). The SREBP/SCAP complex is escorted to the Golgi via COPII proteins where SREBP is released from SCAP and sequentially cleaved by site-1 and site-2 protease, resulting in mature SREBP (mSREBP). mSREBP subsequently translocates to the nucleus, binds to sterol response elements, and transactivates target genes. Recent studies have also identified the PI3K/AKT/mTOR

Authors' Affiliations: Departments of [1]Pathology and Laboratory Medicine, [2]Human Genetics, [3]Neurosurgery, [4]Biomathematics, [5]Institute for Molecular Medicine, [6]Crump Institute for Molecular Imaging, [7]Molecular and Medical Pharmacology, [8]Medicine, David Geffen School of Medicine; [9]Department of Chemistry and Biochemistry, [10]Jonsson Comprehensive Cancer Center, [11]California NanoSystems Institute, University of California, Los Angeles, Los Angeles; [12]Ludwig Institute for Cancer Research; and [13]Moores Cancer Center and [14]Department of Pathology, University of California, San Diego, La Jolla, California

Note: Supplementary data for this article are available at Cancer Research Online (http://cancerres.aacrjournals.org/).

Corresponding Author: Steven Bensinger, University of California, Los Angeles, 36-120 CHS, Box 957278, Los Angeles, CA 90095. Phone: 310-825-9885; Fax: 310-267-6267; E-mail: sbensinger@mednet.ucla.edu

doi: 10.1158/0008-5472.CAN-13-0382-T

AACR *American Association for Cancer Research*

pathway as playing a critical role in driving SREBP activity downstream of receptor tyrosine kinase (RTK) growth receptors in both normal and neoplastic tissue (12–14). Whether SREBPs in cancer cells retain their sterol sensitivity remains controversial (15).

Although it is becoming increasingly clear that heightened SREBP activity is a critical feature of the cancer metabolic program (16–18), the molecular mechanisms by which SREBPs support tumor growth remain poorly delineated. Herein, we show that loss of SREBP1 activity inhibits cancer cell growth and viability, not by globally reducing fatty acid and cholesterol availability, but by uncoupling *de novo* long-chain saturated fatty acid biosynthesis from desaturation. Counterintuitively, we observed that SREBP-inhibited cells maintain significant levels of saturated long-chain fatty acid (16:0 and 18:0) synthesis, despite a clear attenuation of the SREBP-mediated lipid biosynthetic gene program. Isotopomer enrichment studies revealed that SREBP signaling is required to maintain efficient flux of newly synthesized long chain saturated fatty acids into the monounsaturated pool. In the absence of SREBP activity, cancer cells maintain saturated fatty acid synthesis resulting in growth and cellular defects. This defect in fatty acid homeostasis was traced to the maintenance of fatty acid synthase (FASN) activity coupled with the profound loss of stearoyl-CoA desaturase 1 (SCD1) in the absence of SREBP signaling. Replenishing long-chain monounsaturated fatty acids restored significant growth of SREBP-inhibited cells further indicating the role of SREBPs in protecting cells from lipotoxicity. In combination, these studies provide a novel mechanistic explanation for importance of SREBP signaling in the cancer metabolic program and highlight the potential use in targeting the fatty acid desaturation pathway to control tumor growth.

Materials and Methods

Cells, tissue culture, and reagents

U87MG, U251, and T98G cells were provided by Dr. Paul Mischel (Ludwig Institute for Cancer Research, La Jolla, CA). SUM159 cells were provided by Dr. Heather R. Christofk [University of California Los Angeles (UCLA), Los Angeles, CA]. CWR-R1 cells were provided by Dr. Lily Wu (UCLA). U87MG were cultured in Iscove's Modified Dulbecco's Medium (IMDM). These cell lines have not been authenticated. U251 and SUM159 cells were cultured in Dulbecco's Modified Eagle's Medium (DMEM). T98G cells were cultured in DMEM/F12 (50:50) media. CWR-R1 cells were cultured in RPMI. All cell lines were grown in 10% FBS (Omega Scientific) with penicillin/streptomycin (Gibco). Cells were treated with fatostatin (125B11, Chembridge), 25-hydroxycholesterol (25-HC; Sigma), or compound 24 (synthesized at UCLA as described in ref. 19) for 24 hours with respective media containing 1% FBS unless indicated otherwise. Commercial short hairpin RNAs (shRNA) targeting SREBP and SCAP (Sigma) or truncated human SREBP1a (aa 1-490) and SREBP2 (aa 1-484) were used to create stable gain- and loss-of-function cells.

Immunoblots

U87 glioblastoma cells, parental, and genetic constructs were washed once with ice-cold PBS and scraped into radio-immunoprecipitation assay (RIPA) lysis buffer (Boston Bio-Products), with addition of protease and phosphatase inhibitor cocktail (Thermo Fisher Scientific). Equal amounts of protein extracts were separated on gradient 4% to 12% Bis–Tris SDS-PAGE gel (Invitrogen) and then transferred to a nitrocellulose membrane (Amersham). After blocking for 1 hour in a TBS containing 0.1% Tween 20 and 5% nonfat milk, the membrane was probed with indicated antibodies, followed by secondary antibodies conjugated to horseradish peroxidase. The immunoreactivity was revealed by use of an ECL kit (Thermo Fisher Scientific) and autoradiographic film (Genesee Scientific). Antibodies used: anti-SREBP1 and SREBP2 (BD Biosciences), FASN, SCD1, phospho- and total EIF2a, cleaved PARP, and total EIF4E (Cell Signaling).

Gene expression analysis

Cells were collected in TRIzol. Following phenol–chloroform extraction and ethanol precipitation, 700 ng of total RNA were used to synthesize cDNA using the iScript cDNA Synthesis Kit (Bio-Rad) as per manufacturer's instructions. Quantitative PCR (qPCR) was conducted on the Roche Light-Cycler 480 using SYBR Green I Master Mix (Roche) and 0.5 µmol/L primers. Relative expression values are normalized to control gene (36B4) and expressed in terms of linear relative mRNA values. Primer sequences are available upon request.

Proliferation assay

Equal numbers of cells were plated out in separate wells and collected over 5 days of growth. Cells were trypsinized, stained with Trypan Blue (Gibco 15250), and counted on the Nexcelom Cellometer Auto T4. The total number of live cells was calculated for each day of the experiment. For *N*-acetylcysteine rescue assay, 5 mmol/L *N*-acetylcysteine (Sigma) was added to IMDM supplemented with 1% FBS. For oleate rescue assays, oleic acid (Nu-Chek Prep) was conjugated to fatty acid–free bovine serum albumin (BSA; Sigma) in a 7.3:1 molar ratio as previously described (20). Cells were cultured in IMDM supplemented with 1% FBS and 275 µmol/L oleic acid or BSA vehicle. For the cholesterol rescue assay, 1 µg/mL methyl-beta-cyclodextrin-cholesterol (Sigma) was added to IMDM supplemented with 1% FBS.

Cell cycle

Cells were stained to determine DNA content as previously described. Briefly, single cell suspensions were resuspended in a hypotonic staining buffer containing sodium citrate, Triton X-100, ribonuclease A, propidium iodide (PI), and distilled water. Sample was stained for 30 minutes at room temperature and then analyzed by flow cytometry. FACS plots were run using pooled triplicate samples of indicated cell lines.

Xenograft tumor studies

All mice were bred and kept under defined-flora pathogen-free conditions at the Association for Assessment and Accreditation of Laboratory Animal Care-approved Animal Facility of the Division of Experimental Radiation Oncology at the University of California Los Angeles. Mice were handled in accordance with the University of California Los Angeles animal

care policy and approved animal protocols. Nonobese diabetic severe-combined immunodeficient (NOD/SCID)/gamma (NSG) mice (6–12 weeks of age) were implanted subcutaneously in the lower left flank and received a total of 1×10^6 U87 glioma cells. Cells were mixed in a 1:1 ratio with Matrigel matrix (BD Biosciences) and a total volume of 100 μL was injected per mouse. Fatostatin-treated mice received injections of 30 mg/kg intraperitoneally (i.p.) every 3 days. Tumor area was measured by multiplying the length of the tumor (the longest dimension) by the width (the distance perpendicular to the length). For gas chromatography–mass spectrometry (GC-MS) studies on tumor xenografts, tumors were initially resected and weighed. A portion of the tumor weighing 0.1 to 0.15 g was separated, diced, and disrupted by tissue homogenizer in TRIzol. The organic layer of TRIzol extraction was used for mass spectrometry analysis, as described later.

Metabolic pathway-based gene expression enrichment analysis

To identify metabolic pathways associated with both SREBP and SCAP loss-of-function, we used the gene set enrichment analysis (GSEA) algorithm (21) and pathway annotation defined by the Kyoto Encyclopedia of Genes and Genomes metabolic pathways (KEGG; release 44.0; ref. 22). The signal-to-noise ratio (SNR) between the sample classes was used for gene ranking. The metric was calculated for all candidate probesets of each gene and the probeset with maximum absolute metric value was retained. Probeset annotation was based on UniGene build #201 and UniGene identifiers were mapped to each Enzyme Commission number using the gene names provided by KEGG. Pathways with fewer than 3 or greater than 500 nodes represented by the data were excluded from the analysis. This resulted in 92 KEGG metabolic genesets. The classic enrichment statistic was used. Gene-based permutation analysis was used to determine the statistical significance of the results (21).

Metabolic analysis

Cellular metabolic rates were determined by Seahorse Bioanalyzer as described previously (23) with the following modifications. A total of 3×10^5 U87 cells were plated in each well of a V7 plate and allowed to adhere overnight. Mixing, waiting, and measurement times were 2, 2, and 4 minutes, respectively. Drug treatments for oligomycin, carbonyl cyanide 4-(trifluoromethoxy)phenylhydrazone (FCCP), and rotenone–myxothiazol were 0.75 μm/0.25 μm/0.5 μm, respectively.

GC-MS analysis

Cells were cultured in a 1:1 ratio of ^{13}C glucose tracer ([U-^{13}C]-D-glucose; Cambridge Isotope Laboratories) to naturally occurring glucose. Following glucose tracer treatment, cells were collected, washed in PBS, counted, and collected in 500 μL TRIzol. Calibration curves were made using cholesterol, trimyristin, tripalmitin, tripalmitolein, tristearin, and triolein (Nu-Chek Prep) in 500 μL TRIZOL. Internal standards were added to TRIzol suspension; 22 μg of Triheptadecanoin (Nu-Chek Prep) was used as the internal standard for fatty acids and 50 μg of ergosterol (Sigma) was used as the internal standard

for cholesterol. Two hundred microliter of chloroform was added and the resulting aqueous layer was discarded. Organic layers were saponified for 30 minutes at 70°C after adding 600 μL 30% potassium hydroxide and 600 μL 70% ethanol. Sterols were extracted with 3 mL of petroleum ether and dried under nitrogen. Sterols were derivatized to the trimethylsilyl ether form by dissolving in 50 μL N,O-bis(trimethylsilyl) trifluoroacetamide with trimethylchlorosilane 99:1 (Sigma) and 50 μL pyridine followed by 20 minutes at 70°C. Remaining lipid extract was acidified to pH 2 with concentrated hydrochloric acid. Fatty acids were extracted with 3 mL petroleum ether. Extracted fatty acids were derivatized to their methyl ester form with 3 mL methanolic boron trifluoride (Sigma). Fatty acid methyl ester extracts were dried under nitrogen and dissolved in 75 μL ethyl acetate before being run on mass spectrometry.

Data were collected on an Agilent 5975C MSD connected to an Agilent 7890 Gas Chromatograph. Derivitized cholesterol was run on the Phenomenex ZB-MR-1 column (7HG-G016-11). Derivitized fatty acids were run on the Agilent DB-WAX column (122-7032). GC-MS settings and oven programs are available upon request. In unlabeled cells, derivatized cholesterol, myristate (14:0), palmitate (16:0), 16:1 isomers, stearate (18:0), and 18:1 isomers were monitored at m/z 458, 242, 270, 268, 298, and 296, respectively. In labeled cells, they were monitored at m/z 443–490, 240–257, 268–287, 266–285, 296–316, and 294–314, respectively. Derivatized internal standards were monitored at m/z 468 (ergosterol) and 284 (heptadecanoate). Area under curve (AUC) quantitation was conducted on Chemstation software (Agilent).

Fatty acid ratios were determined by dividing the relevant analyte AUC values followed by normalization to controls. Absolute quantitation of lipids was determined by first normalizing the analyte AUC to the internal standard AUC. This ratio was fit to the appropriate calibration curve and then normalized to cell number. In unlabeled samples, M0 only was used to determine the analyte and calibration standard AUC values. In labeled samples, the sum of the AUCs for the molecular ion isotopomers was used. For internal standards, M0 only was used in all cases.

Isotopomer enrichment modeling

Long-chain fatty acids. Determination of *de novo* synthesized fatty acid was determined using a probabilistic model similar to the one developed in refs. 21, 22. The distribution of ^{13}C incorporated into a fatty acid with N total carbons, $L_N(n|q,s,p,e)$, was modeled as a mixture of 2 distributions: synthesized, $C_N(n)$, and nonsynthesized, $B_N(n)$, lipid [Eqs. (1) and (2)]. These distributions are functions of total carbons in the lipid (N), background ^{13}C abundance (q), amount of *de novo* synthesis (s), contribution of label glucose to the cytoplasmic AcCoA pool (p), and ^{13}C enrichment of label glucose (e). Nonsynthesized fatty acids can be simply modeled as a binomial with N trials and success rate q, $B(n|N,q)$. Because synthesized lipids are built using 2-carbon blocks of AcCoA, their distribution is modeled as a sum N/2 i.i.d. 2-carbon-unit distributions. Each 2 carbon unit is modeled as a mixture of 2 binomial distributions, with success rates e for AcCoA originating from glucose, and

q for natural glucose and all other carbon sources [Eq. (2)]. The parameter e is known *a priori* and maximum likelihood estimates (MLE) of q can be calculated from control cell lines grown with no label glucose. The distribution of ^{13}C incorporated, as measured from GC-MS, was used to calculate MLE for p and s in each cell line, replicate, and fatty acid.

$$L_N(q, s, p, e) = s * C_N(q, p, e) + (1 - s) * B(N, q) \qquad (1)$$

$$C_N(q, p, e) = \sum_1^{\frac{N}{2}} [p * B(2, e) + (1 - p) * B(2, q)] \qquad (2)$$

Small corrections were made to account for the possible incorporation of ^{13}C in the methyl ester derivitization of fatty acids.

Cholesterol. Small changes to the above model were made to account for the differences in the synthesis of cholesterol. The carbon contained in *de novo* synthesized cholesterol comes from 10 2-carbon units from AcCoA, and 7 single carbons taken from the AcCoA pool. As earlier, cholesterol labeling is modeled as a sum of nonsynthesized cholesterol, B (27,q), and a sum of i.i.d. distributions defining synthesized cholesterol [Eq. (3)]. Low probability (λ) fragmentation events leading to a loss of 2 mass units is accounted for by modeling the cholesterol distribution as in Eq. (4). Isotopomers of the $[M-15]^+$ fragment were included in the fitting in the event that they overlapped with the molecular ion isotopomers.

$$D(q, s, p, e) = (1 - s) * B(27, q)$$
$$+ s * \left(\sum_1^{10} [p * B(2, e) + (1 - p) * B(2, q)] \right.$$
$$\left. + \sum_1^7 [p * B(1, e) + (1 - p) * B(1, q)] \right) \qquad (3)$$
$$F(\lambda, q, s, p, e) = \lambda * [D(q, s, p, e) - 2]$$
$$+ (1 - \lambda) * D(q, s, p, e) \qquad (4)$$

Small corrections were made for the possible incorporation of ^{13}C, ^{29}Si, and ^{30}Si in the trimethylsilyl ether derivatization of cholesterol.

Results

Cancer cells maintain a sterol sensitive, SCAP-dependent lipogenic program

Brown and Goldstein delineated an elegant lipid-sensitive model of SREBP regulation that is dependent on sterol recognition by the SREBP chaperone proteins INSIG and SCAP (10). More recently, studies have shown that activation of the PI3K/AKT/mTOR signaling pathway also drives SREBP processing and activity (12, 13, 16). However, it remains unclear if SREBP in cancer cells with constitutively activated PI3K/AKT signaling retain sterol-sensitivity and SCAP-dependency. To begin addressing this, we cultured a panel of glioma cells, which have heightened PI3K/AKT signaling (U87, T98G, and U251) with 25-HC, a sterol that binds to SREBP chaperone proteins and inhibits processing. Culturing glioma cells with 25-HC

uniformly inhibited expression of cholesterol and fatty acid biosynthetic genes (Fig. 1A and Supplementary Fig. S1A). Similar results were seen with breast and prostate cancer cells (Supplementary Fig. S1A). We did observe that addition of 25-HC increased SREBP1 gene expression, likely through the transactivation of SREBP1c isoform by the liver X receptors (7). Nevertheless, the observation that 25-HC inhibits SREBP activity indicates that cancer cells retain sterol sensitivity.

Pharmacologic inhibition of SREBP activity with fatostatin (24) or compound 24 (19) resulted in decreased expression of SREBP1 and 2-target genes across an array of glioma, prostate, and breast cancer cell lines (Fig. 1B and Supplementary Figs. S1B and S1C and S2A). Fatostatin and compound 24 also significantly reduced cellular growth (Supplementary Fig. S1D and S1E). The inhibitory activity of 25-HC, fatostatin, and compound 24 on SREBP function is dependent on SCAP (10, 19, 24), suggesting that cancer cells maintain a requirement for SCAP to preserve SREBP signaling. To directly address this, we generated U87 and U251 cells stably expressing shRNAs targeting SREBP1, SREBP2, or SCAP. Real-time reverse transcription PCR (qRT-PCR) and immunoblots confirmed that the knockdown of SCAP markedly attenuated SREBP-target genes (Fig. 1C and Supplementary Fig. S2B–S2E). Treatment of SCAP-deficient cells with compound 24 minimally altered SREBP-target gene expression, indicating maximal loss of SCAP activity in these cells (Supplementary Fig. S2F). Likewise, GSEA confirmed that the loss of SCAP significantly impacts fatty acid and sterol metabolism and is largely confined to those gene sets (Supplementary Table S1). Importantly, loss of SREBP1 or SCAP markedly decreased U87 and U251 glioma cell proliferation *in vitro* (Fig. 1D and Supplementary Fig. S3) characterized by a G_1 cell-cycle arrest (Fig. 1E). Taken together, these data indicate that inhibition of SCAP negatively regulates SREBP-activity and cellular growth in cancer cells irrespective of the heightened PI3K/AKT signaling.

Pharmacologic and genetic inhibition of SCAP attenuates tumor growth

Next, we determined the growth potential of shSREBP1, shSREBP2, or shSCAP U87 xenograft implanted subcutaneously. Knockdown of SREBP1 significantly attenuated tumor growth (Fig. 2A; $P = 0.007$), whereas knockdown of SREBP2 resulted in an intermediate phenotype that did not achieve statistical significance (Fig. 2A). As expected, genetic inhibition of SCAP had the most profound effect on U87 xenograft tumor growth (Fig. 2B; $P < 0.001$). In complementary experiments, we asked if pharmacologic inhibition of SCAP would influence tumor growth *in vivo*. To that end, mice were subcutaneously implanted with parental U87 cells and subsequently treated with fatostatin (5 or 30 mg/kg i.p. every 3 days; ref. 24) starting 3 days after implantation and continuing every 3 days thereafter. Treatment of mice with 30 mg/kg fatostatin significantly reduced U87 xenograft growth (Fig 2C; $P = 0.03$), whereas 5 mg/kg fatostatin attenuated growth approaching statistical significance (Fig. 2C; $P = 0.06$). Taken together, these studies provide proof-of-principle evidence that pharmacologically or genetically targeting SCAP can inhibit SREBP activity and significantly attenuate tumor growth.
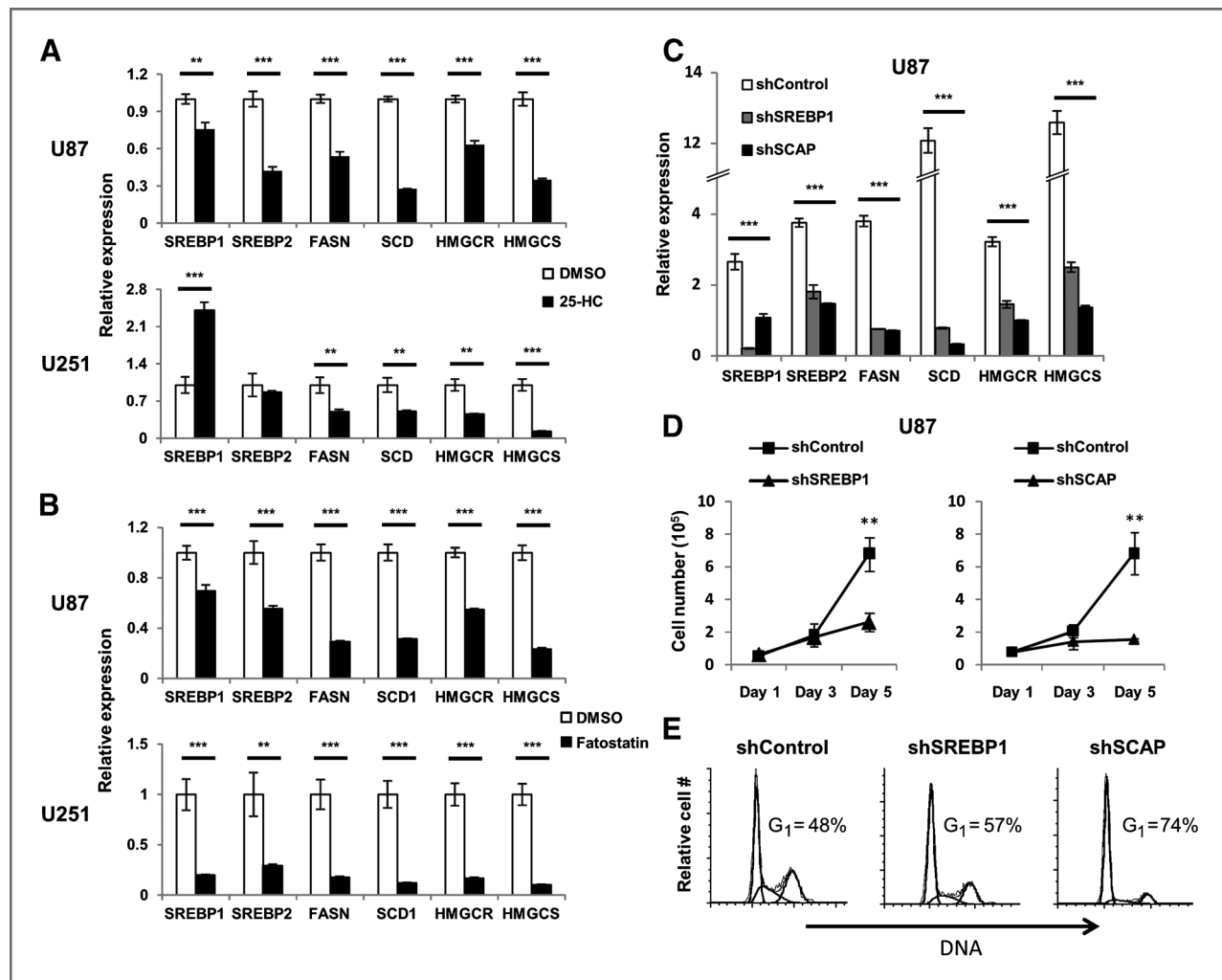
Figure 1. Cancer cells maintain a sterol-sensitive, SCAP-dependent lipogenic program regardless of heightened PI3K/AKT signaling. A and B, SREBP and lipogenic gene expression determined by qPCR in U87 and U251 glioma cells cultured in complete media with 1% serum and treated with 25 µmol/L 25-HC (A) or 10 µmol/L fatostatin (B) for 24 hours. C, SREBP and lipogenic gene expression from U87 cells stably expressing shSREBP1, shSREBP2, or shSCAP cultured in complete media with 1% serum for 24 hours. Growth curve (D) or cell-cycle analysis (E) of U87 cells stably expressing shSREBP1, shSREBP2, or shSCAP U87 cells cultured in complete media with 10% serum. Frequency of cells in G_1 indicated in plot. Cell-cycle plots are representative of $N = 3$ experiments. **, $P < 0.01$; ***, $P < 0.001$.

The SCAP/SREBP axis is not essential to maintain cholesterol homeostasis in glioma cells

Next, we sought to define how SREBP signaling influences cancer cell lipid composition. To that end, control, shSREBP1, and shSCAP cells were cultured for 2 days in complete media with 1% serum to maximize SREBP activity (Supplementary Fig. S4A). Unexpectedly, GC-MS analysis revealed there was no significant difference in cellular cholesterol content between control, shSREBP1, and shSCAP cells (Fig. 3A), despite a clear attenuation of the cholesterol biosynthetic gene program (Fig. 1C). Determination of total cellular cholesterol using colorimetric assays confirmed these minimal changes (Supplementary Fig. S4B). Similar results were seen in SCAP knockdown U251 cells (Fig. 3A). These data suggest that glioma cells can preserve cholesterol content independent of SREBP activity.

Given these surprising results, we asked if SREBP signaling was contributing to cholesterol biosynthesis in U87 cells. To accomplish this, we used a ^{13}C isotopomer enrichment methodology where cells are cultured in 50% mixture of U-^{13}C-glucose for 48 hours (Fig. 3B). The contribution of *de novo* cholesterol synthesis to the total pool was determined by calculating the isotopomer abundances, followed by fitting the data to a probabilistic model (25, 26; see Materials and Methods and Supplementary Fig. S8 for an in-depth explanation). We observed that *de novo* biosynthesis minimally contributes (~1%) to the total cholesterol pool of control U87 cells over a 48-hour labeling period in complete media with 10% serum (Supplementary Fig. S4C). In contrast, placing cells in 1% serum for 48 hours resulted in a 20-fold increase in the contribution of *de novo* cholesterol synthesis to the cellular cholesterol pool (Supplementary Fig. S4C).
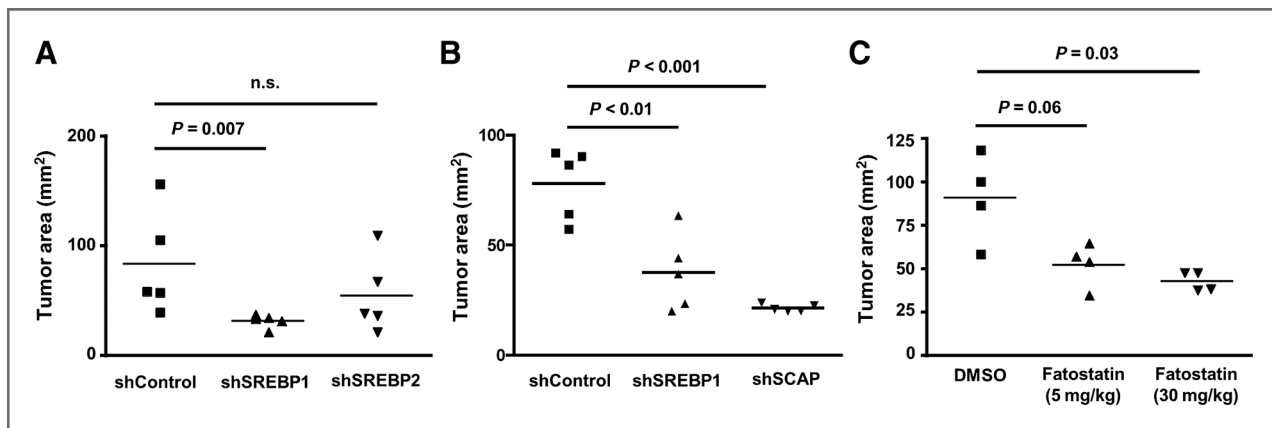
Figure 2. SREBP1 regulates tumor growth. A, tumor area (mm^2) of subcutaneous U87 tumors expressing shSREBP1, shSREBP2, or shControl on day 21. B, tumor area (mm^2) of subcutaneous U87 tumors expressing shSREBP1, shSCAP, or shControl on day 19 postimplantation. C, tumor area (mm^2) of subcutaneous wild-type U87 xenograft on day 21 postimplantation treated with fatostatin (5 or 30 mg/kg) or vehicle i.p. every 3 days. P values indicated on plots.

To determine the contribution of SREBP activity to cholesterol synthesis under low lipid conditions, loss-of-function U87 cells were cultured in complete media and 1% serum containing a 50% mixture of U-^{13}C-glucose for 48 hours. Interestingly, loss of SREBP1 activity decreased *de novo* cholesterol biosynthesis approximately 3-fold (Fig. 3C), consistent with our data that SREBP1 significantly influences the cholesterol synthetic gene program (Fig. 1C). SCAP knockdown nearly ablated the
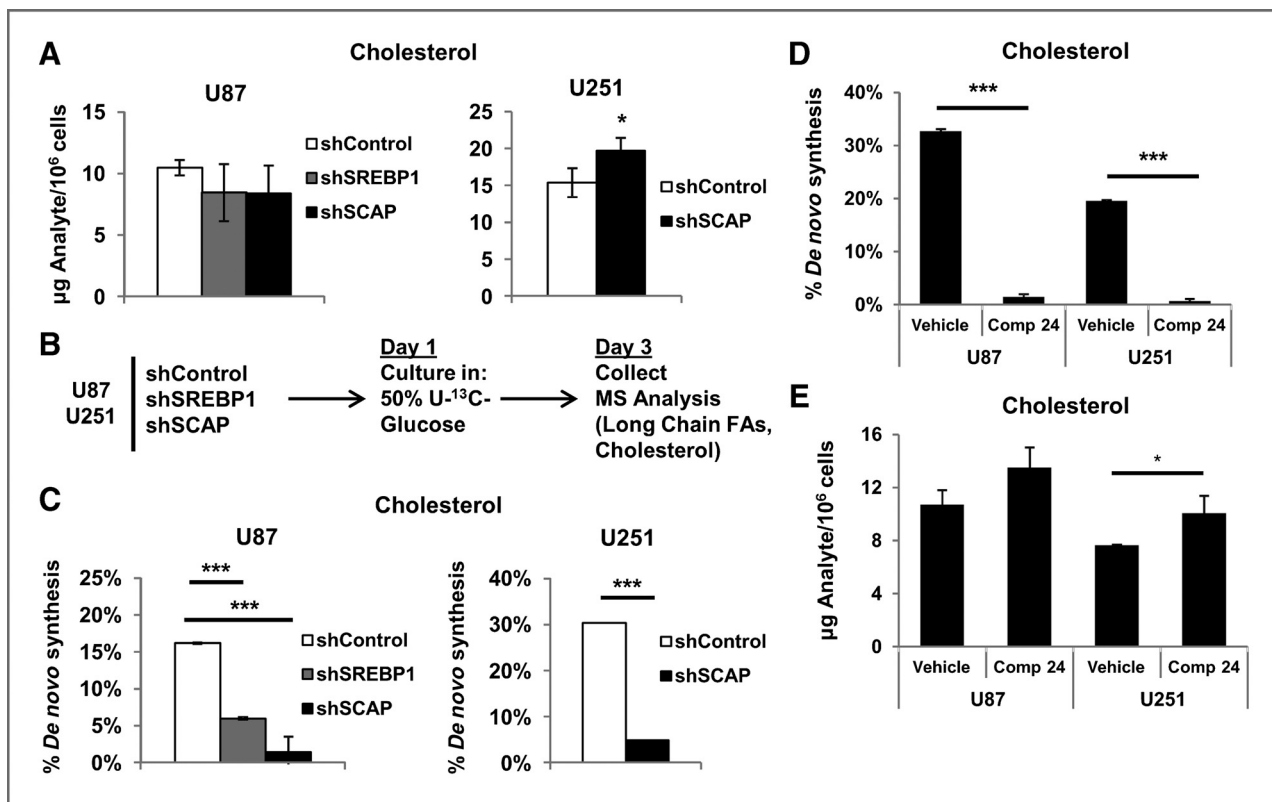

Figure 3. The SCAP/SREBP signaling axis is not required to maintain cholesterol homeostasis in glioma cells. A, GC-MS determination of total cellular cholesterol content of U87 or U251 glioma cells stably expressing shSREBP1, shSREBP2, or shSCAP as indicated cultured in complete media and 1% serum for 48 hours. B, experimental schematic for determination of *de novo* lipid biosynthesis using 50% mixture of U-^{13}C-glucose. C, percentage of cellular cholesterol derived from *de novo* synthesis in U87 or U251 cells stably expressing shSREBP1 or shSCAP cells as indicated and cultured in a 50% mixture of U-^{13}C-glucose and 1% serum for 48 hours. D, percentage of cellular cholesterol derived from *de novo* synthesis in U87 and U251 glioma cells cultured in complete media and 1% serum for 48 hours. Cultures were treated with SREBP inhibitor compound 24 (25 µmol/L) or vehicle. E, total cellular cholesterol content of U87 and U251 cells treated with compound 24 (25 µmol/L) as described earlier for 48 hours. *, $P < 0.05$; ***, $P < 0.001$.

ability of U87 cells to synthesize cholesterol (Fig. 3C), likely as a result of inhibiting SREBP1 and SREBP2 activity. Likewise, U-^{13}C-glucose flux studies conducted on U251 control and SCAP-deficient cells revealed a similar pattern of cholesterol synthesis (Fig. 3C). Despite the influence of SREBP and SCAP on the ability of cells to produce cholesterol in response to low lipid conditions, it is somewhat surprising that total cellular cholesterol content was not grossly affected by stable SREBP inhibition (Fig. 3A)

We were intrigued that loss of SREBP1 or SCAP did not greatly perturb the total cholesterol content of glioma cells and considered the possibility that these results reflected a secondary compensation in knockdown cells. To directly address this, we treated wild-type U87 and U251 cells with compound 24 (19) in 50% mixture of U-^{13}C-glucose and 1% serum for 48 hours. Isotopomer enrichment analysis confirmed that treatment of cells with compound 24 markedly attenuates *de novo* cholesterol biosynthesis (Fig. 3D). Nonetheless, determination of total cellular cholesterol indicated that acute inhibition of SREBP activity in both U87 and U251 cells does not decrease cellular cholesterol content over a 48-hour treatment period (Fig. 3E). Thus, we conclude that glioma cells are capable of maintaining cellular

cholesterol homeostasis independent of significant SREBP activity.

Saturated long-chain fatty acids are maintained in the absence of SREBP activity

Next, we determined the influence of SREBP signaling on cellular long-chain fatty acid composition. Counterintuitively, measurement of long-chain fatty acids revealed that SCAP or SREBP1 knockdown U87 cells cultured in 1% serum for 48 hours showed no change in palmitate (16:0) and an increase in total stearate (18:0; Fig. 4A). In contrast to the total long-chain saturated fatty acids, we observed a marked decrease in the 16:1 and 18:1 monounsaturated fatty acid pools (Fig. 4B). Similar results were seen with U251 loss-of-function cells (Supplementary Fig. S5A). Importantly, the profound loss of monounsaturated long-chain fatty acids (16:1, 18:1) considerably alters the ratio of saturated to monounsaturated fatty acids in cultured glioma cells (Fig. 4C and Supplementary Fig. S5B). Treatment of WT U87 and U251 cells with compound 24 in 1% serum for 48 hours increased total cellular palmitate (16:0) and stearate (18:0) with little or no change in monounsaturated long-chain fatty acids (Fig. 4D). Importantly, the resulting increase in saturated
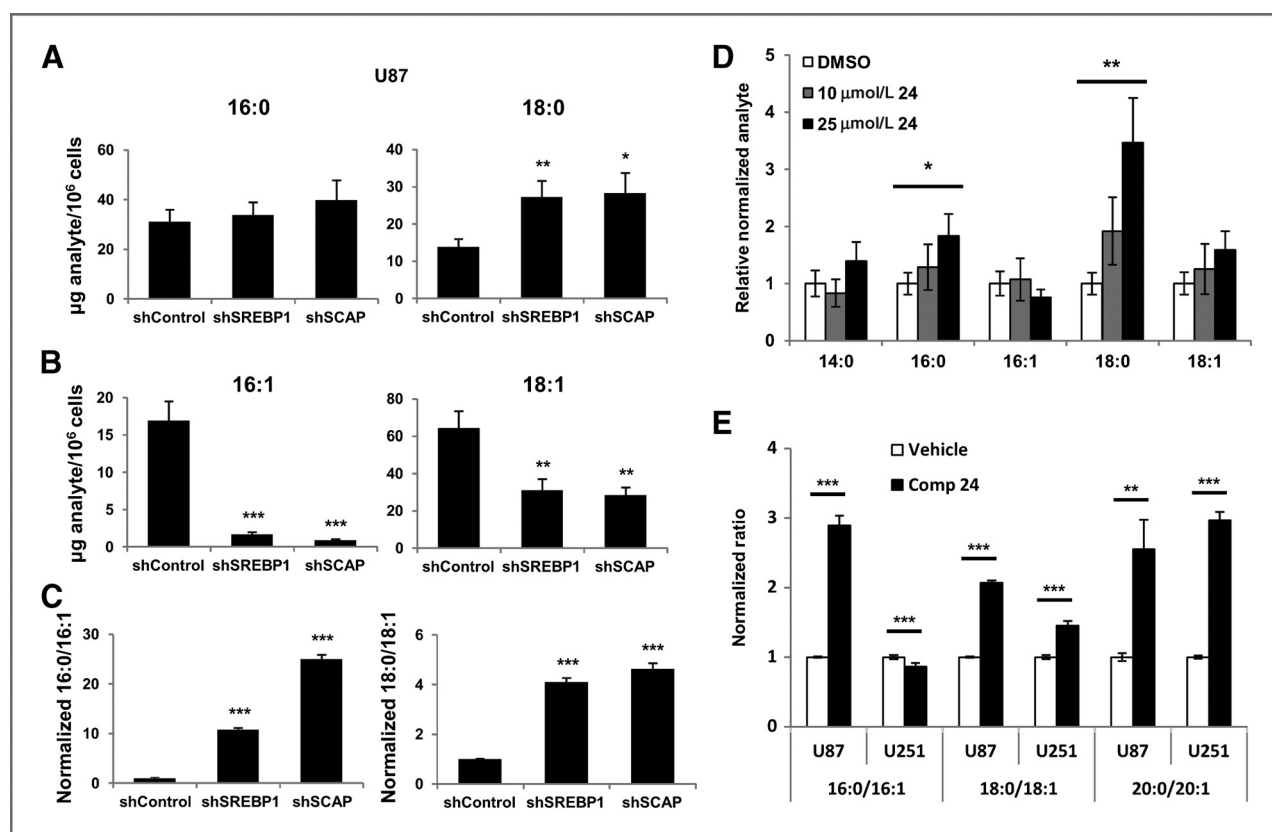

Figure 4. Loss of SREBP results in an increase total saturated long-chain fatty acids. A and B, analysis of total saturated (16:0 and 18:0) and monounsaturated (16:1 and 18:1) long-chain fatty acids from U87 cells stably expressing shSREBP1 or shSCAP. Cells were cultured in complete media and 1% serum for 48 hours. C, determination of the 16:0 to 16:1 and 18:0 to 18:1 ratios in shControl, shSREBP1, or shSCAP cells. D, determination of indicated fatty acids from U87 cells cultured in complete media and 1% serum for 48 hours. In addition, cultures were treated with vehicle or compound 24 (10 or 25 μmol/L) as indicated. E, ratio of 16:0 to 16:1, 18:0 to 18:1 and 20:0 to 20:1 from U87 and U251 cells treated with compound 24 (25 μmol/L) for 48 hours. *, $P < 0.05$; **, $P < 0.01$; ***, $P < 0.001$.

long-chain fatty acids was sufficient to markedly increase the ratio of 16:0 to 16:1, 18:0 to 18:1, and 20:0 to 20:1 in compound 24–treated cells (Fig. 4E), largely phenocopying our genetic models. In combination, our pharmacologic and genetic studies indicate that inhibition of SREBP activity perturbs long-chain fatty acid homeostasis.

SREBPs are required to maintain de novo synthesis of monounsaturated fatty acids

Next, we conducted ^{13}C-isotopomer enrichment studies to determine if the changes in long-chain fatty acid homeostasis in SREBP-inhibited cells were the result of perturbed de novo fatty acid production or from alterations in fatty acid uptake. Surprisingly, analysis of ^{13}C enrichment indicates that loss of SREBP minimally alters de novo synthesis of saturated long-chain fatty acids (Fig. 5A). In contrast to saturated long-chain fatty acids, ^{13}C enrichment in the monounsaturated 16:1 and

18:1 pools was profoundly decreased by the loss of SREBP1 or SCAP (Fig. 5A). Analysis of SCAP-deficient U251 cells revealed a similar pattern of ^{13}C enrichment in the saturated fatty acids and a corresponding decrease in the monounsaturated products (Supplementary Fig. S5C). Determination of ^{13}C enrichment in palmitate and stearate revealed that pharmacologic inhibition of SREBPs activity does significantly attenuate saturated fatty acid biosynthesis (Fig. 5B). However, desaturation of newly synthesized long-chain fatty acids was more sensitive to pharmacologic inhibition of SREBPs (Fig. 5B). Taken together, these results help to explain the changes in the ratio of total saturated to unsaturated long-chain fatty acids observed when SREBPs are genetically or pharmacologically inhibited.

In complementary experiments, we examined the total amounts of saturated and monounsaturated fatty acids in U87 cells ectopically expressing mSREBP1a (designated
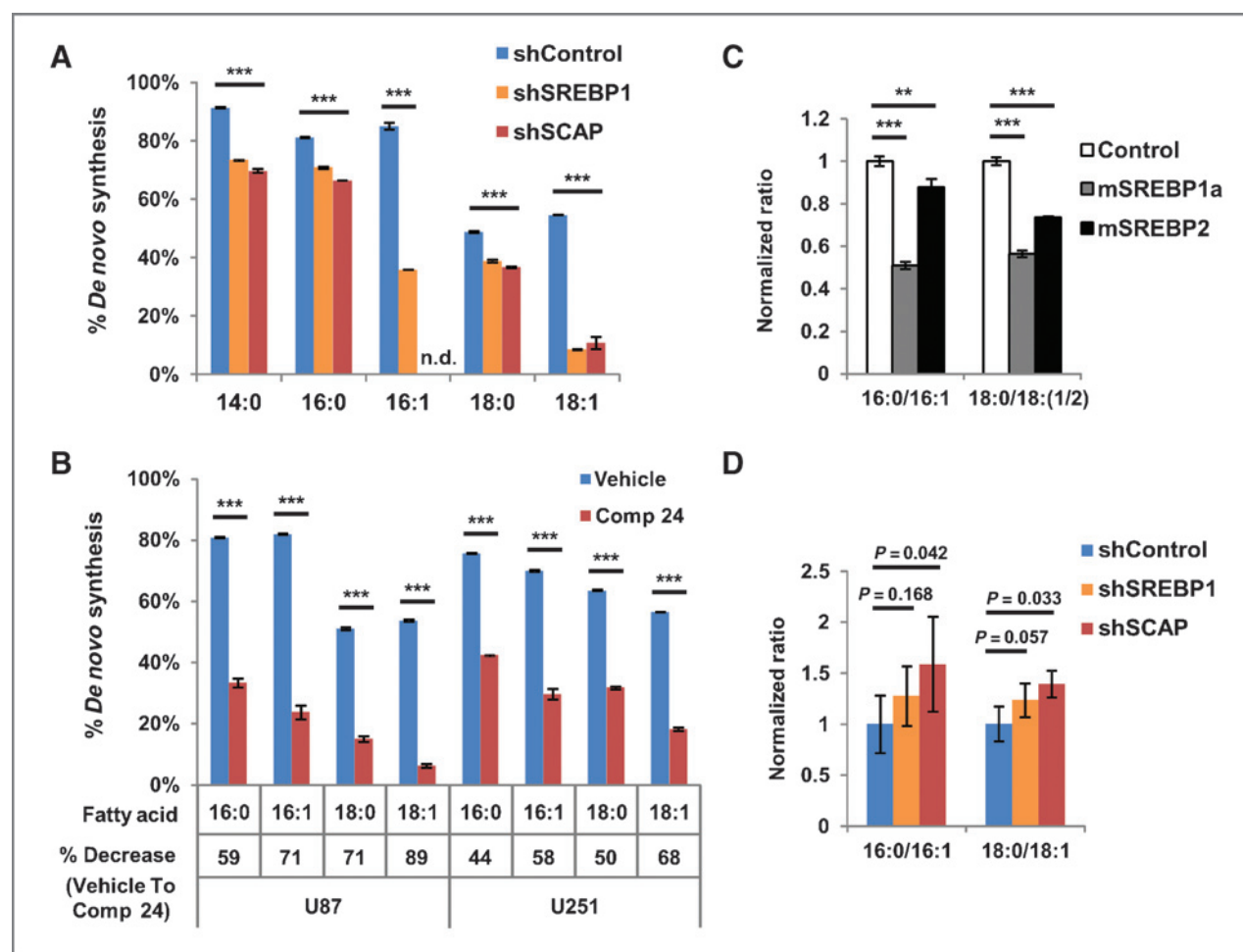

Figure 5. SREBP activity is required to maintain de novo synthesis of monounsaturated fatty acids. A, determination of newly synthesized saturated and monounsaturated fatty acids from U87 cells stably expressing shSREBP1 or shSCAP cultured in complete media containing a 50% mixture of U-^{13}C-glucose and 1% serum for 48 hours. B, percentage of indicated fatty acids derived from de novo synthesis in U87 and U251 glioma cells cultured in complete media containing a 50% mixture of U-^{13}C-glucose and 1% serum for 48 hours. In addition, cultures were treated with vehicle or compound 24 (25 μmol/L) as indicated. C, the ratio of indicated fatty acids from U87 cells stably expressing mSREBP1a, SREBP2 (mSREBP2), or vector control cultured in complete media and 10% serum for 48 hours. D, the ratio of indicated fatty acids from subcutaneous shSREBP1, shSCAP, or shControl U87 xenograft harvested on day 19 postimplantation. **, $P < 0.01$; ***, $P < 0.001$.

mSREBP1; Supplementary Fig. S6A). Not surprisingly, we observed that enforced SREBP1a increased the lipogenic program resulting in a modest increase in total cellular palmitate and stearate (Supplementary Fig. S6B). Despite the increased production of saturated fatty acids, we found that enforced SREBP activity more robustly increased the total 16 and 18 carbon unsaturated fatty acids species (Supplementary Fig. S6B), such that the ratio of saturated to monounsaturated long-chain fatty acids was significantly lower than that of control U87 cells (Fig. 5C). Enforced expression of SREBP2 was able to alter the ratio of saturated to monounsaturated fatty acids (Fig. 5C), albeit to a much lesser extent, indicating that this is more likely a role of SREBP1 in cancer cells.

Next, we asked if SREBP signaling was required to maintain long-chain fatty acid homeostasis in vivo. To that end, control and loss-of-function U87 cells were implanted subcutaneously. Tumors were harvested at an equivalent size and qRT-PCR confirmed the tumors maintained significant knockdowns of SREBP1 or SCAP (Supplementary Fig. S6C). An equivalent mass of tumor for each genotype was used for lipid extraction and subjected to GC-MS to determine long-chain fatty acid content. Strikingly, we observed that the ratio of 16:0/16:1 and 18:0/18:1 was significantly perturbed in SCAP knockdown tumors when compared with control tumors (Fig. 5D). SREBP1 knockdown tumors had a similar alteration in ratios, but did not achieve statistical significance (Fig. 5D). Nevertheless, these data provide compelling evidence that SREBPs signaling is required to preserve long-chain fatty acid homeostasis in cancer cells both in vitro and in vivo.

Loss of SREBP signaling results in lipotoxicity

Alterations in the ratio of saturated to monounsaturated fatty acids can decrease cellular growth via a number of interrelated mechanisms, including perturbations in mitochondrial function, heightened cellular reactive oxygen species (ROS), endoplasmic reticulum stress and apoptosis (27–29). Analysis of mitochondrial function indicates that SCAP-deficient cells have decreased basal oxygen consumption rates (OCR). Sequential treatment of cells with oligomycin (ATPase inhibitor) and FCCP (uncoupling agent) indicated that SCAP knockdown cells have a profound defect in mitochondrial respiratory capacity (Fig. 6A). Analysis of SREBP1 knockdown cells revealed an intermediate phenotype in mitochondrial function (Fig. 6A). These observations led us to ask if ROS homeostasis was also perturbed in loss-of-function cells. Measurement of ROS indicated that both SREBP1- and SCAP-deficient cells had significantly increased ROS (Fig. 6B). Reduction of ROS by the addition of the antioxidant N-acetylcysteine (5 mmol/L) to cultures partially restored proliferative capacity (Supplementary Fig. S7A and S7B; $P < 0.05$,), supporting a role for ROS in negatively regulating growth in this system.
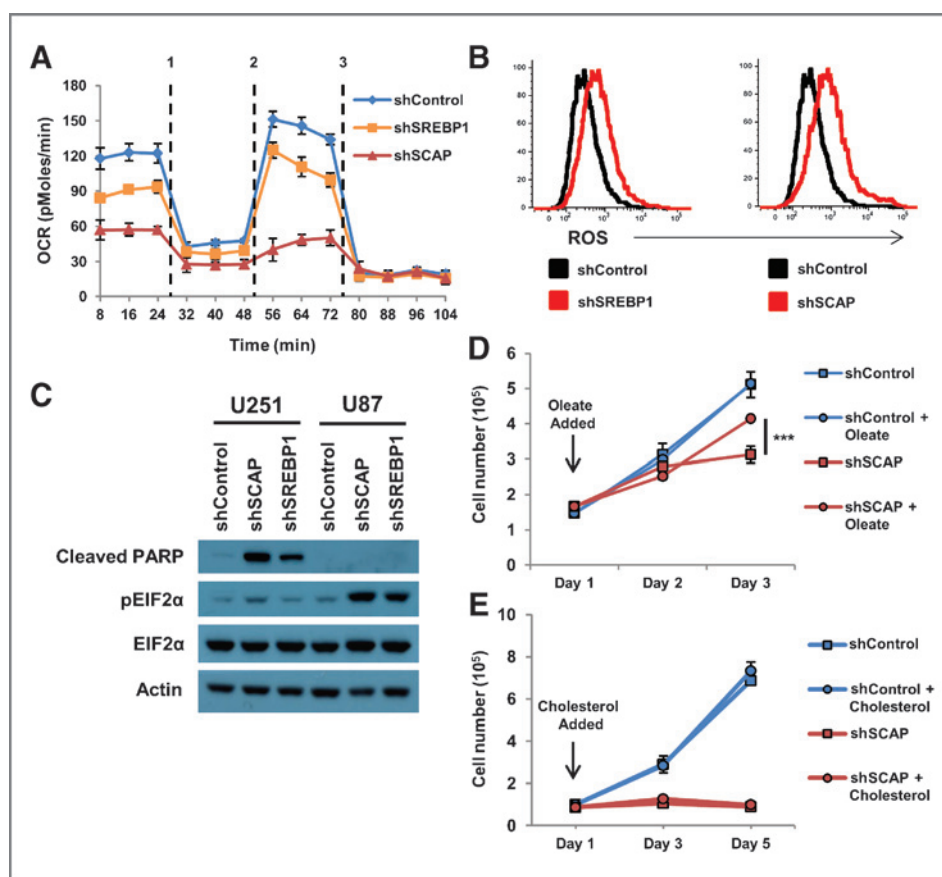

Figure 6. SREBP signaling is required to protect cells from lipotoxicity. A, OCR of U87 SREBP or SCAP knockdown cells in basal state, and in response to sequential treatment with (1) oligomycin (ATPase inhibitor), (2) FCCP (uncoupling agent), and (3) rotenone/myxothiazol (mitochondrial blocker). B, flow-cytometric analysis of cellular ROS levels in shControl, shSREBP1, or shSCAP cells. C, immunoblots assessing phospho- and total EIF2α, cleaved-PARP, and actin from U87 or U251 shControl, shSREBP1, or shSCAP cells as indicated. D, growth curve of shControl or shSCAP U87 cells cultured with 275 μmol/L oleate conjugated to BSA or BSA vehicle. E, growth curve of shControl or shSCAP U87 cells cultured with MBCD-cholesterol (1 μg/mL) or vehicle. ***, $P < 0.001$.

Immunoblots revealed that U87 SREBP1 and SCAP knock-down cells have significantly increased phospho-EIF2α, providing evidence of endoplasmic reticulum stress (Fig. 6C). However, we were unable to detect cleaved-PARP, suggesting no effect of lipotoxicity on apoptosis in these cells (Fig. 6C). In contrast, U251 SREBP and SCAP knockdown cells had significant levels of cleaved-PARP, but minimal p-EIF2α (Fig. 6C). These data indicate that lipotoxicity can have distinct downstream effects even in closely related cell lines, and are consistent with the notion that lipotoxicity can have cell type specific effects (28, 29).

A logical prediction of our data is that replenishing knock-down cells with monounsaturated fatty acids should alleviate cellular dysfunction and restore growth. To test this prediction, we cultured SCAP knockdown cells with exogenous oleate conjugated to BSA and assessed proliferation over 48 hours. Importantly, the addition of oleate significantly restored growth of U87 SCAP-deficient cells without buoying control

cell growth (Fig. 6D). We also considered the possibility that cholesterol was limiting in SCAP-deficient cells. However, providing exogenous cholesterol (MBCD-cholesterol) did not alter the growth of control or SCAP-deficient cells (Fig. 6E). Taken together, these data indicate that SREBP-inhibited cells acquire severe lipotoxicity that can be alleviated by replenishing monounsaturated fatty acid pools.

Loss of SCD1 induces lipotoxicity and phenocopies loss of SREBP1

Finally, we posited that the pleotropic effects on growth and metabolic dysfunction observed in SREBP-inhibited cells could potentially be attributed to loss of SCD1 activity. To test this hypothesis, we generated stable SCD1 knockdown U87 cells. qRT-PCR confirmed loss of SCD1 with little effect on SREBP target gene expression (Supplementary Fig. S7C). Growth curves revealed that loss of SCD1 significantly impacts proliferative capacity (Fig. 7A). GC-MS analysis indicates that
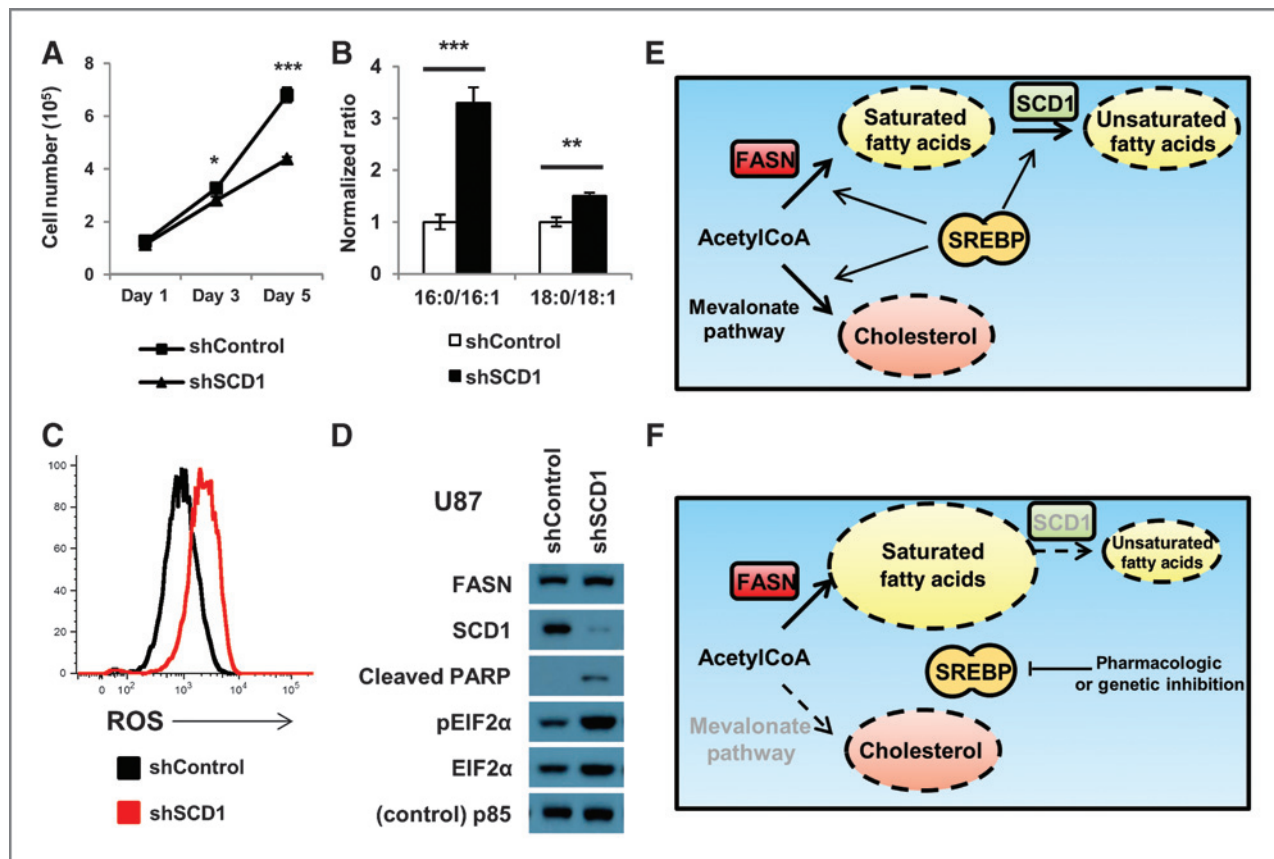

Figure 7. Loss of SCD1 phenocopies loss of SREBP1 in cancer cells. A, growth curve of U87 cells stably expressing shControl or shSCD1 cultured in complete media and 1% serum. B, ratio of indicated saturated to monounsaturated long-chain fatty acids determined by GC-MS in control and SCD1 knockdown U87 cells cultured in complete media and 1% serum for 48 hours. C, flow-cytometric analysis of cellular ROS levels in control or shSCD1 cells cultured as earlier. D, immunoblots assessing FASN, SCD1, phospho-, and total EIF2α, and cleaved-PARP from U87 control or shSCD1 cells cultured in complete media and 1% serum for 24 hours. E, a model for the mechanism by which SREBPs protect from lipotoxicity. Under low sterol or monounsaturated fatty acid conditions, SREBPs are transcriptionally active coordinating *de novo* saturated fatty acid production with de saturation through the regulation of SCD1. Likewise, *de novo* cholesterol biosynthesis is driven by the upregulation of genes involved in the mevalonate pathway. F, when SCAP or SREBP1 are inhibited, cells compensate for the loss of *de novo* cholesterol synthesis by increased scavenging of cholesterol or decreased efflux in an SREBP-independent manner. Importantly, SREBP-inhibited cells maintain saturated fatty acid production, but cannot desaturate these products due to a loss of SCD1 activity. Uncoupling saturated fatty acid synthesis from desaturation alters the ratios of these fatty acids resulting in profound lipotoxicity. **, $P < 0.01$; ***, $P < 0.001$.

loss of SCD1 altered the ratio of 16:0/16:1 and 18:0/18:1 with no change in cellular cholesterol content (Fig. 7B and Supplementary S7D). Correspondingly, we observed heightened ROS (Fig. 7C) and phosphorylation of EIF2α indicative of endoplasmic reticulum stress and lipotoxicity (Fig. 7C and D). Taken together, these data support the notion that SREBPs influence tumor growth and viability in an SCD1-dependent manner, and highlight the requirement for coordinated regulation of fatty acid biosynthesis with desaturase activity.

Discussion

The lipogenic program of cancer cells has emerged as an important component of the cancer metabolic phenotype (30). However, the molecular events underlying the transcriptional control of lipid anabolism in cancer remains poorly defined. The SREBPs have a well-established role in the transcriptional control of lipid biosynthesis (7, 8). Thus, we posited that SREBP1 and 2 signaling would influence lipid anabolism and tumor growth. Consistent with this notion, we find a strong dependence on SREBP1 activity to maintain cancer cell proliferation and tumor growth. We also find that SREBP2 contributes to tumor growth, but to a lesser extent than SREBP1. Using a combination of genetic and pharmacologic models, we also show that inhibition of the SREBP chaperone protein SCAP provides a robust and efficient method for antagonizing both SREBP1 and SREBP2 proteins. More significantly, our data provide an important proof-of-concept that targeting SCAP can be a viable approach for perturbing the cancer metabolic program and attenuating tumor growth.

Although our studies clearly support the developing paradigm that SREBPs are essential for cancer cell growth and tumorigenesis (31), we were surprised to find that inhibition of SREBP did not significantly decrease the cellular pool of saturated fatty acids. Using isotopomer enrichment techniques, we were able to trace this surprising and counterintuitive result to the uncoupling of saturated fatty acid production from desaturation. Although it has been presumed that SREBP1 is essential for lipogenesis, our observation that cancer cells continue to synthesize significant levels of palmitate and stearate indicates that FASN activity in cancer cells can be SREBP1 independent. In stark contrast, the Δ9 desaturation of newly synthesized long-chain fatty acids seems to be exquisitely reliant on SREBP activity. Thus, our data suggest that SREBP1 signaling is essential to ensure coordination between de novo fatty acid synthesis and desaturation, rather than general fatty acid anabolism. The result of uncoupling FASN and SCD1 activity via inhibition of SREBPs in tumor cells is the aberrant accumulation of newly synthesized saturated fatty acids (e.g., palmitate and stearate). This accumulation results in a dramatic alteration in the ratio of saturated to monounsaturated fatty acids (see model-Fig. 7E) and ensuing cellular dysfunction, or lipotoxicity. On the basis of the results of our studies, we would hypothesize that the difference between a tumor's long-chain fatty acid synthetic rate and its Δ9 desaturase activity may serve as an important stratification method for identifying tumors susceptible to SREBP or SCD inhibitors.

As to why perturbations in the ratio of saturated to unsaturated long-chain fatty acids have such a profound effect on cellular growth or survival remains poorly understood. One potential explanation is that the aberrant synthesis of saturated fatty acids perturbs the composition of newly synthesized phospholipids in the endoplasmic reticulum bilayer. Incorporation of phospholipids with an excess of saturated fatty acid moieties would result in significant changes to the biophysical properties of the newly synthesized membranes in the endoplasmic reticulum. Altering endoplasmic reticulum membrane function could initiate an endoplasmic reticulum stress response by engaging components of the unfolded protein response (UPR; ref. 32). As such, the fatty acid synthetic program of a cancer cell directly links phospholipid homeostasis with protein synthesis, and consequently impacts the assembly or function of cellular organelles and the plasma membrane. A second interrelated component of lipotoxicity is the excessive production of ceramide, a bioactive lipid molecule implicated in an array of cellular processes including apoptosis (33). Ceramide is enzymatically produced in the endoplasmic reticulum through a series of steps initiated via the condensation of palmiate and serine by serine-palmitoyl transferase. Finally, mitochondrial dysfunction and excessive ROS production feed into endoplasmic reticulum stress and apoptotic pathways (28, 29). For reasons that remain unclear, responses to lipotoxicity are cell type specific. Thus, the response of cancers to aberrant lipid accumulation will likely be heterogeneous and we provide evidence that two distinct glioma lines have disparate responses to loss of monounsaturated fatty acids.

We were also quite surprised to find that loss of SREBP activity did not greatly alter cellular cholesterol content. Analysis of ^{13}C isotope enrichment in cholesterol revealed that glioma cells synthesize little of their total cellular cholesterol when lipid is freely available in the serum. Moving cells into low lipid conditions resulted in a significant upregulation of de novo cholesterol biosynthesis, confirming that glioma cells can retain a lipid responsive metabolic program. Determination of ^{13}C isotope enrichment in the cholesterol compartment of SREBP loss-of-function cells showed that the upregulation in cholesterol biosynthesis is SREBP-dependent. Nevertheless, mass spectrometry studies indicate that SREBP-inhibited glioma cells are able to maintain cellular cholesterol homeostasis, indicating strong compensatory mechanisms for the loss in synthetic capacity. We hypothesize that heightened scavenging likely plays a dominant role in this process, although we cannot rule out other compensatory mechanisms such as decreased cholesterol export.

Importantly, these studies help to explain why pharmacologic inhibition of the mevalonate (or de novo synthetic) pathway with statins has been met with variable success (34). The capacity of glioma cells to maintain homeostasis without SREBP suggests that targeting cholesterol-scavenging pathways would be a far more efficient approach to depriving cells of cholesterol. In support of this notion, recent work by Guo and colleagues showed a critical role for low-density lipoprotein (LDL) receptor mediated uptake of lipoproteins in the preservation of cholesterol homeostasis and tumor

growth. In these studies, activation of the liver X receptor drove expression of the E3 ligase IDOL resulting in degradation of LDLR and reduced tumor growth (35). Our isotopomer studies indicating that cholesterol scavenging is the dominant method in achieving required cholesterol content provide a mechanistic explanation as to why perturbations in lipoprotein scavenging would be so critical for glioma tumor growth and survival.

In conclusion, the data presented herein reveal an unexpected requirement for SREBP signaling in protecting cancer cells from aberrant accumulation of saturated fatty acids and lipotoxicity. Moreover, these studies provide proof-of-principle evidence that targeting SREBP regulatory proteins, such as the SREBP chaperone protein SCAP, could provide a viable therapeutic approach for the regulation of SREBP activity in tumors. Finally, our studies raise the intriguing possibility that infusions of ^{13}C glucose into tumor bearing patients followed by biopsy and mass spectrometry could provide an important opportunity to identify lipid metabolic vulnerabilities that could be therapeutically exploited.

Disclosure of Potential Conflicts of Interest

P.S. Mischel is a consultant/advisory board member of Celgene. No potential conflicts of interest were disclosed by the other authors.

Authors' Contributions

Conception and design: K.J. Williams, J.P. Argus, A.G. York, L.M. Liau, S.J. Bensinger

Development of methodology: K.J. Williams, J.P. Argus, M.Q. Wilks, B.N. Marbois, D.N. Lisiero, R.M. Prins, S.J. Bensinger
Acquisition of data (provided animals, acquired and managed patients, provided facilities, etc.): K.J. Williams, J.P. Argus, Y. Zhu, B.N. Marbois, Y. Kidani, A.L. Pourzia, D. Akhavan, D.N. Lisiero, A.H. Henkin, B.T. Chamberlain, L. Vergnes, M.E. Jung, L.M. Liau, R.M. Prins, K. Reue, S.J. Bensinger
Analysis and interpretation of data (e.g., statistical analysis, biostatistics, computational analysis): K.J. Williams, J.P. Argus, Y. Zhu, M.Q. Wilks, B.N. Marbois, Y. Kidani, A.L. Pourzia, D.N. Lisiero, E. Komisopoulou, L. Vergnes, J.Z. Torres, R.M. Prins, P.S. Mischel, T.G. Graeber, S.J. Bensinger
Writing, review, and/or revision of the manuscript: K.J. Williams, J.P. Argus, M.Q. Wilks, L.M. Liau, H.R. Christofk, R.M. Prins, P.S. Mischel, T.G. Graeber, S.J. Bensinger
Administrative, technical, or material support (i.e., reporting or organizing data, constructing databases): J.P. Argus, H. Soto
Study supervision: H. Soto, S.J. Bensinger

Acknowledgments

Grant Support

References

1. Hanahan D, Weinberg RA. Hallmarks of cancer: the next generation. Cell 2011;144:646–74.
2. Warburg O. On the origin of cancer cells. Science 1956;123:309–14.
3. Gatenby RA, Gillies RJ. Why do cancers have high aerobic glycolysis? Nat Rev Cancer 2004;4:891–9.
4. DeBerardinis RJ, Lum JJ, Hatzivassiliou G, Thompson CB. The biology of cancer: metabolic reprogramming fuels cell growth and proliferation. Cell Metab 2008;7:11–20.
5. DeBerardinis RJ, Mancuso A, Daikhin E, Nissim I, Yudkoff M, Wehrli S, et al. Beyond aerobic glycolysis: transformed cells can engage in glutamine metabolism that exceeds the requirement for protein and nucleotide synthesis. Proc Natl Acad Sci U S A 2007;104:19345–50.
6. Wise DR, DeBerardinis RJ, Mancuso A, Sayed N, Zhang XY, Pfeiffer HK, et al. Myc regulates a transcriptional program that stimulates mitochondrial glutaminolysis and leads to glutamine addiction. Proc Natl Acad Sci U S A 2008;105:18782–7.
7. Horton JD, Goldstein JL, Brown MS. SREBPs: activators of the complete program of cholesterol and fatty acid synthesis in the liver. J Clin Invest 2002;109:1125–31.
8. Horton JD, Shah NA, Warrington JA, Anderson NN, Park SW, Brown MS, et al. Combined analysis of oligonucleotide microarray data from transgenic and knockout mice identifies direct SREBP target genes. Proc Natl Acad Sci U S A 2003;100:12027–32.
9. Hsu PP, Sabatini DM. Cancer cell metabolism: Warburg and beyond. Cell 2008;134:703–7.
10. Goldstein JL, DeBose-Boyd RA, Brown MS. Protein sensors for membrane sterols. Cell 2006;124:35–46.
11. Radhakrishnan A, Goldstein JL, McDonald JG, Brown MS. Switch-like control of SREBP-2 transport triggered by small changes in ER cholesterol: a delicate balance. Cell Metab 2008;8:512–21.
12. Porstmann T, Santos CR, Griffiths B, Cully M, Wu M, Leevers S, et al. SREBP activity is regulated by mTORC1 and contributes to Akt-dependent cell growth. Cell Metab 2008;8:224–36.
13. Li S, Brown MS, Goldstein JL. Bifurcation of insulin signaling pathway in rat liver: mTORC1 required for stimulation of lipogenesis, but not inhibition of gluconeogenesis. Proc Natl Acad Sci U S A 2010; 107:3441–6.
14. Duvel K, Yecies JL, Menon S, Raman P, Lipovsky AI, Souza AL, et al. Activation of a metabolic gene regulatory network downstream of mTOR complex 1. Mol Cell 2010;39:171–83.
15. Krycer JR, Kristiana I, Brown AJ. Cholesterol homeostasis in two commonly used human prostate cancer cell-lines, LNCaP and PC-3. PLoS ONE 2009;4:e8496.
16. Guo D, Prins RM, Dang J, Kuga D, Iwanami A, Soto H, et al. EGFR signaling through an Akt-SREBP-1-dependent, rapamycin-resistant pathway sensitizes glioblastomas to antilipogenic therapy. Sci Signal 2009;2:ra82.
17. Ettinger SL, Sobel R, Whitmore TG, Akbari M, Bradley DR, Gleave ME, et al. Dysregulation of sterol response element-binding proteins and downstream effectors in prostate cancer during progression to androgen independence. Cancer Res 2004;64:2212–21.
18. Heemers H, Verrijdt G, Organe S, Claessens F, Heyns W, Verhoeven G, et al. Identification of an androgen response element in intron 8 of the sterol regulatory element-binding protein cleavage-activating protein gene allowing direct regulation by the androgen receptor. J Biol Chem 2004;279:30880–7.
19. Kamisuki S, Shirakawa T, Kugimiya A, Abu-Elheiga L, Choo HY, Yamada K, et al. Synthesis and evaluation of diarylthiazole derivatives that inhibit activation of sterol regulatory element-binding proteins. J Med Chem 2011;54:4923–7.
20. Van Harken DR, Dixon CW, Heimberg M. Hepatic lipid metabolism in experimental diabetes. V. The effect of concentration of oleate on metabolism of triglycerides and on ketogenesis. J Biol Chem 1969; 244:2278–85.
21. Subramanian A, Tamayo P, Mootha VK, Mukherjee S, Ebert BL, Gillette MA, et al. Gene set enrichment analysis: a knowledge-based approach

for interpreting genome-wide expression profiles. Proc Natl Acad Sci U S A 2005;102:15545–50.

22. Kanehisa M, Araki M, Goto S, Hattori M, Hirakawa M, Itoh M, et al. KEGG for linking genomes to life and the environment. Nucleic Acids Res 2008;36:D480–4.

23. Vergnes L, Chin R, Young SG, Reue K. Heart-type fatty acid-binding protein is essential for efficient brown adipose tissue fatty acid oxidation and cold tolerance. J Biol Chem 2011;286:380–90.

24. Kamisuki S, Mao Q, Abu-Elheiga L, Gu Z, Kugimiya A, Kwon Y, et al. A small molecule that blocks fat synthesis by inhibiting the activation of SREBP. Chem Biol 2009;16:882–92.

25. Kelleher JK, Masterson TM. Model equations for condensation biosynthesis using stable isotopes and radioisotopes. Am J Physiol 1992;262:E118–25.

26. Metallo CM, Gameiro PA, Bell EL, Mattaini KR, Yang J, Hiller K, et al. Reductive glutamine metabolism by IDH1 mediates lipogenesis under hypoxia. Nature 2012;481:380–4.

27. Inoguchi T, Li P, Umeda F, Yu HY, Kakimoto M, Imamura M, et al. High glucose level and free fatty acid stimulate reactive oxygen species production through protein kinase C–dependent activation of NAD(P)H oxidase in cultured vascular cells. Diabetes 2000;49:1939–45.

28. Alkhouri N, Dixon LJ, Feldstein AE. Lipotoxicity in nonalcoholic fatty liver disease: not all lipids are created equal. Expert Rev Gastroenterol Hepatol 2009;3:445–51.

29. van de Weijer T, Schrauwen-Hinderling VB, Schrauwen P. Lipotoxicity in type 2 diabetic cardiomyopathy. Cardiovasc Res 2011;92:10–8.

30. Menendez JA, Lupu R. Fatty acid synthase and the lipogenic phenotype in cancer pathogenesis. Nat Rev Cancer 2007;7:763–77.

31. Shao W, Espenshade PJ. Expanding roles for SREBP in metabolism. Cell Metab 2012;16:414–9.

32. Schroder M, Kaufman RJ. The mammalian unfolded protein response. Annu Rev Biochem 2005;74:739–89.

33. Ogretmen B, Hannun YA. Biologically active sphingolipids in cancer pathogenesis and treatment. Nat Rev Cancer 2004;4:604–16.

34. Clendening JW, Penn LZ. Targeting tumor cell metabolism with statins. Oncogene 2012;31:4967–78.

35. Guo D, Reinitz F, Youssef M, Hong C, Nathanson D, Akhavan D, et al. An LXR agonist promotes glioblastoma cell death through inhibition of an EGFR/AKT/SREBP-1/LDLR-dependent pathway. Cancer Discov 2011;1:442–56.